
White Rose Research Online

eprints@whiterose.ac.uk
https://eprints.whiterose.ac.uk
Universities of Leeds, Sheffield and York

Deposited via The University of Sheffield.

White Rose Research Online URL for this paper:
https://eprints.whiterose.ac.uk/id/eprint/124483/

Version: Accepted Version

Article:
Kumar, A. and De Souza, M.M. (2018) Modelling the threshold voltage for p-channel E-mode GaN HFETs. IET Power Electronics, 11 (4). ISSN: 1755-4535

https://doi.org/10.1049/iet-pel.2017.0438

Reuse
Items deposited in White Rose Research Online are protected by copyright, with all rights reserved unless indicated otherwise. They may be downloaded and/or printed for private study, or other acts as permitted by national copyright laws. The publisher or other rights holders may allow further reproduction and re-use of the full text version. This is indicated by the licence information on the White Rose Research Online record for the item.

Takedown
If you consider content in White Rose Research Online to be in breach of UK law, please notify us by emailing eprints@whiterose.ac.uk including the URL of the record and the reason for the withdrawal request.


UNIVERSITY OF LEEDS
University of Sheffield
UNIVERSITY of York

Modelling the Threshold Voltage for p-channel E-mode GaN HFETs

Ashwani Kumar [1*] and Maria Merlyne De Souza[1†]

[1] Department of Electronic and Electrical Engineering, University of Sheffield, George Porter Building, Broad Lane, Sheffield, United Kingdom
[*]akumar4@sheffield.ac.uk; [†]m.desouza@sheffield.ac.uk

Abstract: ***P-channel GaN Metal Oxide Semiconductor Heterostructure Field Effect Transistors (MOSHFETs) utilising a polarization induced two Dimensional Hole Gas (2DHG) operate inherently in depletion mode (D-mode). The condition for their conversion to E-mode operation is examined via analytical expressions for the threshold voltage and verified via TCAD simulations. Between the two heterostructures (i) conventional GaN/AlGaN/GaN and (ii) alternate AlGaN/GaN/AlGaN/GaN examined in this work, we demonstrate at higher threshold voltage ($> |-2|\ V$), the alternate heterostructure can potentially achieve a higher on-current by a factor of 2 of ($\sim 30\ mA/mm$), without degradation in the on-off current ratio, expected ideally to be of the order of ~ 12.***

1. Introduction

Spontaneous polarisation and piezoelectric strain along the [0001] orientation are main contributors to the high density of two dimensional sheet electron density ($>10^{13} cm^{-2}$) at an interface of AlGaN/GaN in GaN High Electron Mobility Transistors (HEMTs). Due to the high mobility of electrons, this two dimensional electron gas (2DEG) leads to high performance power and frequency applications [1–3], that have contributed to GaN being considered one of the fastest growing semiconductors today [4]. Similarly, a negative polarization charge at the GaN/AlGaN heterointerface can generate a two dimensional hole gas (2DHG), which behaves as a semiconducting field plate for effective control of electric field crowding at the gate edge of power devices [5]. This 2DHG has more recently, sparked interest towards realization of p-channel GaN heterostructure field effect transistors (p-HFETs), necessary for implementing power converter systems on a chip [6].

Despite a low mobility of holes in wurtzite GaN, $\sim 16\ cm^2/Vs$ [7–9], because of a high density 2DHG of $\sim 5 \times 10^{13}\ cm^{-2}$, p-channel HFETs with a maximum on-current $|I_{ON}|$ of $150\ mA/mm$ in depletion mode (D-mode) were demonstrated by Li *et al.* in [10]. Nevertheless, it is precisely this high density that makes it difficult to deplete, and resulted in an on-off current ratio of ~ 1 order in magnitude for this device. For realising an enhancement mode (E-mode) p-channel HFET with a high $|V_{th}|$, a low density of the 2DHG of $\sim 6 \times 10^{11}\ cm^{-2}$ led to a degradation in on-current by two orders of magnitude [11]. The maximum on-current for enhancement-mode (E-mode) p-channel HFETs reported experimentally to date, lies in the range of $0.3 - 10\ mA/mm$ [10–12], with a maximum reported $|V_{th}|$ of $|-1.3|\ V$ [12]. Nevertheless, an E-mode p-channel HFET with a $|V_{th}|$ of $|-1|\ V$ to $|-2|\ V$ is desirable for integrated gate drivers for fail-safe operation of power management integrated circuits (PMICs) [13].

The current work consolidates our understanding of the mechanisms of achieving effective high $|V_{th}|$ in p-channel HFETs in GaN on a polarisation superjunction platform that is fully compatible with power device fabrication [5]. An analytical expression for the $|V_{th}|$ in terms of material parameters and geometry is demonstrated for two potential candidate structures for p-channel E-mode operation, described as (i) a conventional heterostructure without an AlGaN cap and (ii) an alternate heterostructure with an AlGaN cap, that was shown to provide additional flexibility for addressing the trade-off between the $|V_{th}|$ and on-current by us in [14]. The expressions proposed in this work may be easily used in back-of-envelope calculations to design the V_{th} by adjusting the Al mole fraction in the AlGaN cap layer.

2. Methodology

The structures examined in this work are simulated via TCAD modelling of the Poisson equation coupled with carrier continuity [15]. Shockley-Read-Hall and Augur recombination are employed to model trap kinetics. The low field mobility is described by the Albrecht model [16] whereas a nitride specific field dependent model is used under high field [17]. The maximum hole mobility at room temperature is limited to $16\ cm^2/V \cdot s$ [18], while a contact resistance ρ_c of $10^{-4}\ \Omega cm^2$ is used for source and drain contacts to p-GaN [19].

The conventional and alternate heterostructures (without and with an AlGaN cap) are presented in Figs. 1 (a) & (b), respectively. The conventional structure from bottom to the top, consists of a GaN buffer, AlGaN barrier, and GaN channel layers, all grown along the [0001] direction, as shown in Fig. 1 (a) with an additional gated oxide layer at the top, with the GaN buffer in a relaxed state. Due to the lattice mismatch between AlGaN and GaN, a strain is developed within AlGaN barrier layer, during its pseudomorphic growth upon the buffer. The lattice constant a_0 for AlGaN, with an Al mole fraction x is estimated by linearly interpolating between the lattice constants for GaN and AlN, which are typically 3.189 Å and 3.112 Å [20]. Thus the strain in AlGaN can be described as $\left(a_{0,AlGaN} - a_{0,GaN}\right)/a_{0,GaN} \approx 2.4x$ %.

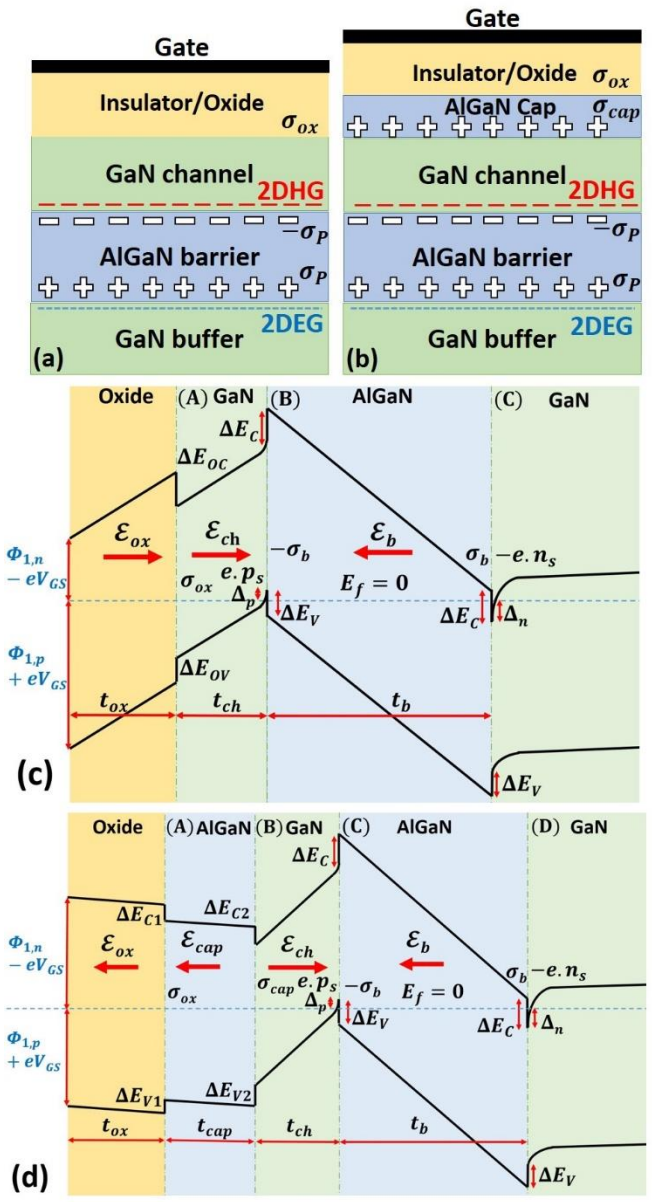

Fig. 1. *Schematic cross-sections beneath the gate of the conventional and alternate heterostructures (without and with AlGaN cap respectively) and corresponding band diagrams.*
(a) Conventional heterostructure from top to bottom consisting of oxide/insulator, undoped GaN channel, AlGaN barrier, and GaN buffer layers, (b) Alternate heterostructure from top to bottom consisting of oxide/insulator, AlGaN cap layer, undoped GaN channel, AlGaN barrier, and GaN buffer layers, (c) Energy band diagrams of the conventional heterostructure, (d) Energy band diagrams of the alternate heterostructure

Since AlGaN is lattice matched to the GaN buffer, the GaN channel layer above the AlGaN remains relaxed. Owing to strain induced piezoelectric polarization and the difference in spontaneous polarization, a polarization sheet charge density σ_b is created at the bottom and top interfaces of AlGaN. In the alternate heterostructure an additional strain is developed within the AlGaN cap on top of the relaxed GaN channel, which depends upon the Al mole fraction in the cap layer. As a result of the polarization difference between the AlGaN cap and channel layer, an additional polarization sheet charge density σ_{cap} is created along the cap/channel interface in Fig. 1 (b). By adjusting the Al mole fraction in the cap layer σ_{cap} can be modified, providing an additional handle in either controlling or depleting the 2DHG in the GaN channel under the gate.

The schematic band diagrams for the two heterostructures displayed in Figs. 1 (c) & 1 (d), emphasize the distinct features, such as conduction and valence band offsets at the interfaces of oxide/GaN and AlGaN/GaN heterointerfaces, and the electron and hole quantum wells that are not easily obvious in simulated band diagrams. In deriving an expression for V_{th}, a procedure similar to that employed by H. Hahn *et al.* in [21] is adopted. In this approach, first the charge densities at various interfaces are evaluated by the application of Gauss' Law under the electrostatic constraints introduced by the heterostructure. The electron or hole densities are substituted to zero to obtain the gate bias which is defined as the threshold voltage. While deriving the threshold voltage, it is assumed that the 2DEG is grounded via the source terminal. This allows saturated device characteristics, since previously it has been shown that a floating 2DEG leads to non-saturation of the I-V curves [22]. This mechanism distinguishes the device from that reported in [23]. Moreover, the thicknesses of GaN channel and AlGaN cap layers are sufficiently small to prevent formation of any undesirable electron or hole quantum wells at any of the interfaces between the oxide, GaN channel, and the AlGaN cap layers.

2.1. Conventional Heterostructure

Following the valence band in Fig. 1 (c) and moving from the gated surface of the oxide on the left to the interface of the GaN channel/AlGaN barrier, marked as (B), on the right, the energy relative to the Fermi level E_f can be written as

$$-\frac{\Phi_{1,p}}{e} - V_{GS} + t_{ox}\mathcal{E}_{ox} + \frac{\Delta E_{OV}}{e} + t_{ch}\mathcal{E}_{ch} = \frac{\Delta_p}{e} \qquad (1)$$

where $\Phi_{1,p}$ is the barrier height of the valence band at the gate/oxide interface, ΔE_{OV} is the valence band offset between the oxide and GaN channel, t_{ox} and t_{ch} are thicknesses of the oxide and GaN channel respectively, $\mathcal{E}_{ox}$ and $\mathcal{E}_{ch}$ represent the electric field within the oxide and GaN channel layers, respectively, and Δ_p is the height of the hole quantum well (QW). Applying Gauss' law at interfaces (A) and (B), respectively, leads to

$$\epsilon_{ch}\mathcal{E}_{ch} - \epsilon_{ox}\mathcal{E}_{ox} = \sigma_{ox} \qquad (2)$$

$$\epsilon_{ch}\mathcal{E}_{ch} + \epsilon_b\mathcal{E}_b = \sigma_b - e \cdot p_s \qquad (3)$$

where ϵ_{ox}, ϵ_{ch}, and ϵ_b are the permittivities of oxide, GaN channel, and AlGaN barrier layers, $\mathcal{E}_b$ is the electric field within the barrier layer, σ_{ox} is the unpassivated sheet charge or net sheet charge density along the oxide and channel interface, σ_b is the net polarization sheet charge density between the GaN channel and AlGaN barriers at interface (B), and p_s represents the density of 2DHG. It can be inferred from Fig. 1 (c), that for both hole and electron quantum wells (QWs) (Δ_n & Δ_p) to simultaneously exist, the electric field within the AlGaN barrier must be large enough to provide a band bending equivalent to the energy of the bandgap of GaN (E_G) over the thickness of the barrier t_b, which can be expressed as

$$t_b \mathcal{E}_b \approx \frac{E_G}{\mathrm{e}} \tag{4}$$

In order to eliminate the explicit electric field dependence in (2) and (3), first $\mathcal{E}_b$ is substituted from (4) into (3)

$$\epsilon_{ch}\mathcal{E}_{ch} = \sigma_b - e \cdot p_s - C_b \frac{E_G}{e} \tag{5}$$

where $C_b = \epsilon_b / t_b$ is the unit area capacitance associated with the barrier layer. Rewriting (2) by substituting $\epsilon_{ch}\mathcal{E}_{ch}$ from (5) gives

$$\epsilon_{ox}\mathcal{E}_{ox} = \sigma_b - \sigma_{ox} - e \cdot p_s - C_b \frac{E_G}{e} \tag{6}$$

Finally, the dependence of the electric field in (1) can be eliminated by substituting $\mathcal{E}_{ch}$ from (5) and $\mathcal{E}_{ox}$ from (6), which results in

$$V_{GS} = \left(\sigma_b - e \cdot p_s - C_b \frac{E_G}{e}\right)\left(\frac{1}{C_{ox}} + \frac{1}{C_{ch}}\right) - \frac{\sigma_{ox}}{C_{ox}} - \frac{\Phi_{1,p}}{e} + \frac{\Delta E_{OV}}{e} - \frac{\Delta_p}{e} \tag{7}$$

Where $C_{ox}(= \epsilon_{ox}/t_{ox})$ and $C_{ch}(= \epsilon_{ch}/t_{ch})$ are the unit area capacitances in the oxide and channel layers. Defining $C_{oc} = (1/C_{ox} + 1/C_{ch})^{-1}$ as the equivalent unit area capacitance offered by the oxide and channel layers, and following the definition of threshold voltage as the gate bias at which the height of the hole QW Δ_p must be zero and $e \cdot p_s$ should be negligibly small compared to σ_b [21], (7) can be expressed as

$$V_{th} = \frac{\sigma_b}{C_{oc}} - \frac{C_b}{C_{oc}}\frac{E_G}{e} - \frac{\sigma_{ox}}{C_{ox}} - \frac{\Phi_{1,p}}{e} + \frac{\Delta E_{OV}}{e} \tag{8}$$

From (8), it can be inferred that a higher polarization charge at the GaN channel and AlGaN barrier heterointerface drives the threshold voltage upwards, i.e. a D-mode regime. Moreover, an increase in barrier thickness (i.e. reduction of C_b) means a relatively smaller band bending across the barrier required for the formation of both electron and hole quantum wells simultaneously, driving the device towards a D-mode regime. A detailed description of the impact of the other parameters is presented in the subsequent section.

2.2. Alternate Heterostructure with an AlGaN cap

A similar procedure can be followed to obtain an expression of the V_{th} in the heterostructure with the AlGaN cap layer (Fig. 1 (b)). Here we present only the key steps while highlighting important differences. Considering the band diagram in Fig. 1 (d), the variations of energy of the valence band, as before, can be represented as

$$-\frac{\Phi_{1,p}}{e} - V_{GS} - t_{ox}\mathcal{E}_{ox} + \frac{\Delta E_{V1}}{e} - t_{cap}\mathcal{E}_{cap} + \frac{\Delta E_{V2}}{e} + t_{ch}\mathcal{E}_{ch} = \frac{\Delta_p}{e} \tag{9}$$

Where t_{cap} is the thickness of the AlGaN cap layer,$\mathcal{E}_{cap}$ is the electric field within this layer, ΔE_{V1} and ΔE_{V2} are valence band offsets at the interfaces of oxide/cap and cap/channel, respectively, $\Delta E_{V1} + \Delta E_{V2} = \Delta E_{OV}$, the net valence band offset between the oxide and GaN channel, as in the conventional structure. Moreover, as opposed to (1), the term $t_{ox}\mathcal{E}_{ox}$ in (9) bears a negative sign. This is owing to the fact that in this heterostructure, there is an additional polarization sheet charge density σ_{cap}, introduced by the AlGaN cap layer, which is responsible for a change in the direction of electric field in the oxide layer [14]. An application of Gauss' law at the interfaces (A), (B), and (C) gives

$$\epsilon_{ox}\mathcal{E}_{ox} - \epsilon_{cap}\mathcal{E}_{cap} = \sigma_{ox} \tag{10}$$

$$\epsilon_{cap}\mathcal{E}_{cap} + \epsilon_{ch}\mathcal{E}_{ch} = \sigma_{cap} \tag{11}$$

$$\epsilon_{ch}\mathcal{E}_{ch} + \epsilon_b\mathcal{E}_b = \sigma_b - e \cdot p_s \tag{12}$$

Where ϵ_{cap} is the dielectric constant of the AlGaN cap layer. Equation (4) is still applicable in the barrier layer, as long as the band bending is sufficient to form both electron and hole QWs simultaneously. Employing equations (4) and (10)-(12) to remove the electric field dependence in (9), leads to

$$V_{GS} = \left(\sigma_b - e \cdot p_s - C_b \frac{E_G}{e}\right)\left(\frac{1}{C_{ox}} + \frac{1}{C_{cap}} + \frac{1}{C_{ch}}\right) - \sigma_{cap}\left(\frac{1}{C_{ox}} + \frac{1}{C_{cap}}\right) - \frac{\sigma_{ox}}{C_{ox}} - \frac{\Phi_{1,p}}{e} + \frac{\Delta E_{OV}}{e} - \frac{\Delta_p}{e} \tag{13}$$

Where $C_{cap}(= \epsilon_{cap}/t_{cap})$ is the unit area capacitance offered by the AlGaN cap layer. Defining $C_{occ} = \left(1/C_{ox} + 1/C_{cap} + 1/C_{ch}\right)^{-1}$, $C_{ocp} = \left(1/C_{ox} + 1/C_{cap}\right)^{-1}$, and at $V_{GS} = V_{th}$ substituting, Δ_p as zero as well as assuming $e \cdot p_s$ to be negligible in comparison with σ_b, (13) reduces to the desired expression as

$$V_{th} = \frac{\sigma_b}{C_{occ}} - \frac{C_b}{C_{occ}}\frac{E_G}{e} - \frac{\sigma_{cap}}{C_{ocp}} - \frac{\sigma_{ox}}{C_{ox}} - \frac{\Phi_{1,p}}{e} + \frac{\Delta E_{OV}}{e} \tag{14}$$

(14) is similar to (8) except for the additional term $-\sigma_{cap}/C_{ocp}$ which results from the additional polarization sheet charge introduced by the AlGaN cap layer that helps bring V_{th} down to the desired negative levels for a p-channel device. In order to compare the predicted threshold voltage from (8) and (14) with simulated results, all the parameters in the equations are kept same as mentioned in the user manual of the TCAD [24]. These parameters along with the polarization charge model are summarised in Table 1.

Table 1. *Parameters used in the calculation of the threshold voltage from equations (8) and (14) for the two heterostructures examined in this work*

Parameters	Values
$\Phi_{1,p}\ (eV)$	4.9
$\Delta E_{OV}\ (eV)$	2.15
$E_G\ (eV)$	3.43
$\epsilon_{ox}\ (Al_2O_3)$	$9.3\epsilon_0$
ϵ_{ch}	$8.9\epsilon_0$
ϵ_b or $\epsilon_{cap}\ (Al_xGa_{1-x}N)$	$8.5x\epsilon_0 + 8.9(1-x)\epsilon_0$
$\sigma_{ox}\ (oxide/GaN)$	$0.1\sigma_b$
$\sigma_{ox}\ (oxide/AlGaN)$	$0.1\sigma_{cap}$
σ_b or $\sigma_{cap} = \lvert\Delta P_{sp}\rvert + \lvert\Delta P_{pz}\rvert$	
$P_{sp}\ (GaN)\ (C/m^2)$	-0.034
$P_{sp}\ (Al_xGa_{1-x}N)\ (C/m^2)$	$-0.09x - 0.034(1-x)$
$P_{pz}\ (Al_xGa_{1-x}N) = 2\frac{a(x)-a_0}{a_0}\left(e_{31} - \frac{C_{13}}{C_{33}}e_{33}\right)$	
$a_0\ (Å)\ (GaN)$	3.189
$a\ (Al_xGa_{1-x}N)\ (Å)$	$3.112x + 3.189(1-x)$
$e_{33}\ (Al_xGa_{1-x}N)\ (C/m^2)$	$1.5x + 0.67(1-x)$
$e_{31}\ (Al_xGa_{1-x}N)\ (C/m^2)$	$-0.53x - 0.34(1-x)$
$C_{13}\ (Al_xGa_{1-x}N)\ (GPa)$	$127x + 100(1-x)$
$C_{33}\ (Al_xGa_{1-x}N)\ (GPa)$	$382x + 392(1-x)$

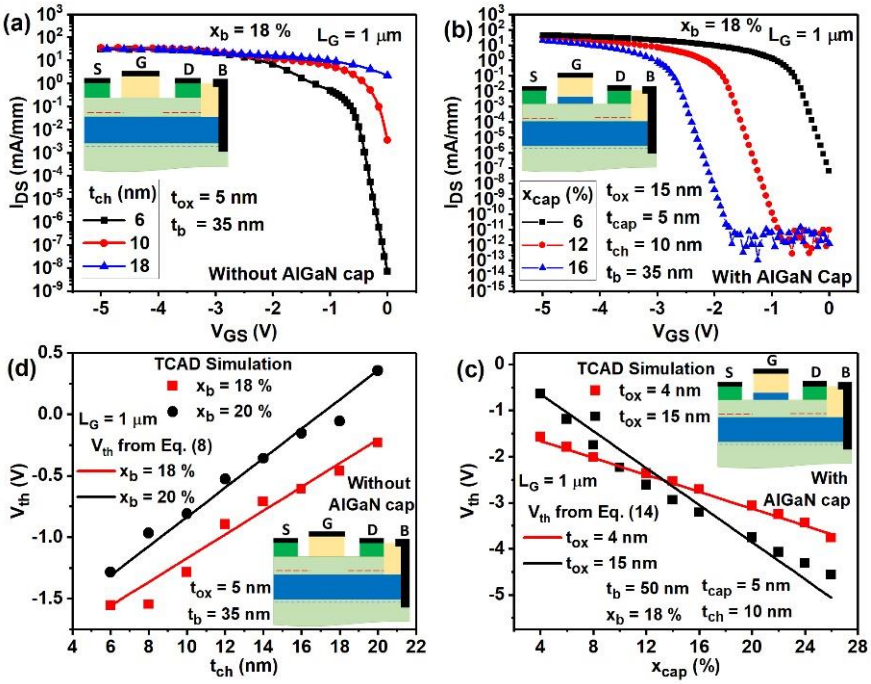

Fig. 2. *Transfer characteristics for the two heterostructures and validation of the expression for* V_{th} *via TCAD simulations using the* g_{max} *method for the p-channel MOSHFETs with gate length of* 1 μm*, for two heterostructures.*
(a) $I_{DS} - V_{GS}$ characteristics in a conventional heterostructure at different channel thickness t_{ch}, (b) $I_{DS} - V_{GS}$ characteristics in an alternate heterostructure at different Al mole fraction in the AlGaN cap x_{cap}, (c) Comparison of V_{th} *vs.* t_{ch} for the conventional heterostructure at different Al mole fractions in the barrier x_b from simulation and Equation (8), (d) Comparison of V_{th} *vs.* x_{cap} in the alternate heterostructure with a channel thickness of 10 nm and an AlGaN cap at different oxide thicknesses t_{ox} from simulation and Equation (14)

3. Results and Discussions

The derived threshold voltage expressions are verified with the threshold voltage extracted from the simulated transfer characteristics for the two heterostructures shown in Figs. 2 (a) and (b). In Figs. 2 (c) and (d), the predicted threshold voltage from (8) and (14) are compared with the threshold voltage obtained from the simulated transfer characteristics, where Al_2O_3 is used as the gate dielectric in all the results. As seen from the device geometries in the inset, an additional base contact, marked B, is employed here to keep the 2DEG connected to ground. V_{th} is extracted from the simulated transfer characteristics, by drawing a tangent to the drain current corresponding to a maximum transconductance g_{max} in the transfer characteristics on a linear scale and checking its intercept at the axis of the gate bias (g_{max} method).

In the case of the conventional structure in Fig. 2 (c), the threshold voltage from the model, plotted as a function of thickness of the channel layer, for two distinct Al mole fractions in the barrier layer is in the good agreement with the simulated results.

As opposed to the p-channel MOSFET in Si, $|V_{th}|$ of this device improves as the thickness of the channel is reduced. This contrasting behaviour is a result of the direction of the electric field between the gate and the 2DHG, as marked by the arrows in Fig. 1 (c), which is opposite in GaN to that of a p-channel MOSFET in Si. A reduction in the Al mole fraction in the barrier lowers the polarization sheet charge density, which in turn leads to a reduction in the density of 2DHG. Hence, an improvement in $|V_{th}|$ is observed with a reduction in x_b, as seen in Fig. 2 (c). This behaviour of $|V_{th}|$ with a change in either t_{ch} or x_b has also been demonstrated experimentally in p-channel HFETs [11, 12].

For the alternate structure with the AlGaN cap from Fig. 2 (d), $|V_{th}|$ of the device becomes higher as the Al mole fraction in the AlGaN cap layer is increased. The figure also shows a cross-over point between the curves at different t_{ox}, which corresponds to x_{cap} in the range of $10 - 14\%$, below which the device behaves similar to a conventional structure i.e. a smaller $|V_{th}|$ at higher t_{ox}. An increase in x_{cap} beyond the cross-over point leads to an increase in the polarization sheet charge at the interface of the AlGaN cap/GaN channel which causes the electric field in the oxide and the cap layer to now point towards the gate (Fig. 1 (d)), resulting in an increased $|V_{th}|$ at higher t_{ox}. To find out the polarization sheet charge density in the cap layer corresponding to the cross-over $\sigma_{cap,co}$, we can solve for $\epsilon_{ox}\mathcal{E}_{ox}$ utilising (4), (10), (11), & (12) while assuming a negligible density of hole gas, which leads to

$$\epsilon_{ox}\mathcal{E}_{ox} = \sigma_{ox} + \sigma_{cap} - \sigma_b + C_b\frac{E_G}{e} \qquad (15)$$

The electric field within the oxide at the cross-over value of σ_{cap} must vanish. Hence substituting $\mathcal{E}_{ox}$ in (15) to zero, yields

$$\sigma_{cap,co} = \sigma_b - \sigma_{ox} - C_b\frac{E_G}{e} \qquad (16)$$

This change in the behaviour of threshold voltage with the oxide thickness at higher x_{cap} is also apparent in Fig. 3, which compares the threshold voltage obtained from

Equations (8) and (14) with a variation in t_{ox}. For the conventional structure, $|V_{th}|$ always reduces with an increase in t_{ox} and depends only upon the charges at different interfaces without being affected by the thicknesses of the oxide or channel. For the AlGaN cap structure, at small x_{cap} the device shows a decrease in $|V_{th}|$ as t_{ox} becomes larger. However, as x_{cap} becomes greater than $\sim 12\%$, which corresponds to cross-over value of polarization charge density in the cap $\sigma_{cap,co}$, as defined in (16), the behaviour of $|V_{th}|$ *vs.* t_{ox} in the alternate structure becomes opposite to that observed in the conventional one.

Results from Fig. 2 (c) and Fig. 3 for the conventional structure indicate that a reasonable level of V_{th} ($\sim -1.5\ V$) can be obtained either by reducing the thicknesses of oxide and channel layers to $< 8\ nm$ and x_b ($\sim 18\ \%$), which can put considerable strain on manufacturing processes particularly due to the control of Mg doping required. A reduction in t_{ch} and t_{ox} increases the electrical field along the vertical direction and causes a higher gate leakage current, while a reduction in x_b lowers the polarization charge, necessary for producing a high density of 2DHG, thus resulting in a degradation in the on-current. In contrast, the threshold voltage in the alternate structure is not restricted by these limitations. By adjusting the x_{cap} in the AlGaN cap layer, the term σ_{cap}/C_{ocp} in (14), can be altered to produce a sufficiently large V_{th}. Moreover, once σ_{cap} is higher than its cross-over value in (16), a thicker oxide layer can be used to further increase the $|V_{th}|$.

Figs. 4 (a) & (b) show the on-current (defined as drain to source current at $-5\ V$ of V_{GS} and V_{DS}) and on-off current ratio with respect to change in the threshold voltage for p-channel MOSHFETs with both structures ($L_G = 1\ \mu m$). In the case of the conventional structure, the threshold voltage is varied by changing the Al mole fraction in the AlGaN barrier layer, while in the AlGaN cap structure, the V_{th} is controlled by adjusting the Al mole fraction in AlGaN cap with x_b kept fixed at $\sim$23%, as shown.

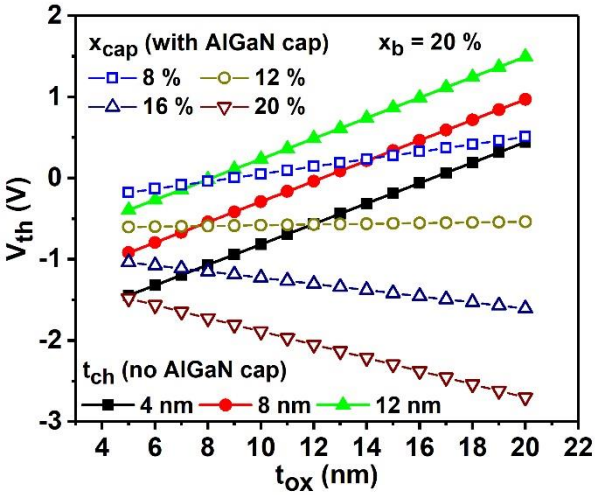

Fig. 3. *A comparison of threshold voltage vs. oxide thickness t_{ox} at different channel thicknesses t_{ch} for the heterostructure without AlGaN cap, and at different Al mole fractions in the cap x_{cap} in the heterostructure with AlGaN cap and a channel thickness of* 10 *nm.*

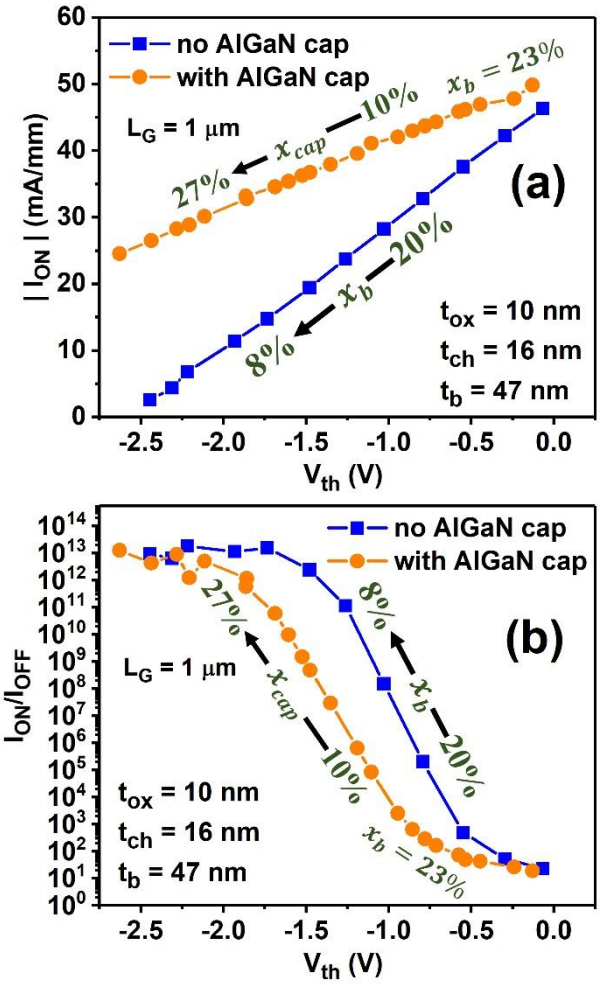

Fig. 4. *Comparison of electrical performance of p-channel MOSHFETs with and without the AlGaN cap layer as a function of threshold voltage.*
(a) On-current $|\boldsymbol{I_{ON}}|$ *vs.* threshold voltage $\boldsymbol{V_{th}}$, (b) On-Off current ratio $\boldsymbol{I_{ON}/I_{OFF}}$ *vs.* threshold voltage $\boldsymbol{V_{th}}$

With an increase in $|V_{th}|$ in Fig. 4 (a), the on-current reduces, as expected in a conventional device, due to the overall reduction in the density of 2DHG in all regions including the access regions. For the alternate structure, an increase in x_{cap} depletes the 2DHG only under the gate, thus not affecting the series resistance of the access regions of the contacts. Thus, $|I_{ON}|$ drops more sharply with the increase in $|V_{th}|$ for the conventional device.

On-off current ratio, which we have defined as the ratio of the currents in the on-state ($V_{GS} = -5\ V$) and off-state ($V_{GS} = 0\ V$) of a normally-off p-channel device, shows a rise by orders of magnitude with an increase in $|V_{th}|$ in Fig. 4 (b). Since the devices do not turn-off completely when V_{th} is close to $0\ V$, hence a poor on-off current ratio of $\sim$1 is observed. As $|V_{th}|$ increases, a higher on-off current ratio in the conventional structure arises from a smaller off-current or leakage current due to a low density of 2DHG. Additionally, the gate retains better electrostatic control in modulating the charge density in the channel giving an I_{ON}/I_{OFF} $\sim$3 order of magnitude higher compared to the AlGaN cap device for V_{th} in the range of $[-0.75, -1.5]\ V$. However, at even higher $|V_{th}|, > |-2.0|\ V$, a higher polarization charge introduced by the AlGaN cap layer effectively depletes the 2DHG under the

gate, thus suppressing the off-current, which results in both the devices showing a similar on-off current ratio.

4. Conclusion

The threshold voltage characteristics of two candidate GaN heterostructures for p-type devices in GaN are examined with the help of analytical threshold voltage expressions derived in this work. The threshold voltage equation for the conventional heterostructure reveals that a sufficiently negative level of threshold voltage, which comes at the expense of employing ultrathin oxide and channel layers while reducing Al mole fraction in the AlGaN barrier layer. These methods however can increase the leakage and degrade the device performance. An alternate heterostructure is explored as a solution to these issues, which consists of an additional AlGaN cap layer on top of GaN channel. The derived threshold voltage equation for this geometry proves that this heterostructure can potentially achieve higher $|V_{th}|$ by adjusting the Al mole fraction in the AlGaN cap layer. The simulation results indicate that the trade-off present between threshold voltage and the on-current is weaker in the device with AlGaN cap, thereby resulting an on-current of $\sim 30\ mA/mm$ at $|V_{th}|$ of $|-2|\ V$, which is more than double than that achievable in the device without the AlGaN cap layer. While the on-off current ratio for the AlGaN cap structure remains lower at threshold voltage below $|-2|\ V$, it shows an improvement with an increase in the $|V_{th}|$, becoming equivalent to the one achieved for a conventional heterostructure without AlGaN cap, $\sim 10^{12}$, at $|V_{th}|$ of greater than $|-2|\ V$.

5. Acknowledgement

The authors acknowledge funding from ENIAC-JU program E2SG for partial support of this research.

6. References

[1] Mishra, U.K., Shen, L., Kazior, T.E.: 'GaN-based RF power devices and amplifiers'*Proc. IEEE*, 2008, **96**, (2), pp. 287–305.

[2] Shibata, D., Kajitani, R., Ogawa, M., *et al.*: '1.7 kV/1.0 mΩcm 2 normally-off vertical GaN transistor on GaN substrate with regrown p-GaN/AlGaN/GaN semipolar gate structure', in '2016 IEEE International Electron Devices Meeting (IEDM)' (IEEE, 2016), p. 10.1.1-10.1.4

[3] Saadat, O.I., Chung, J.W., Piner, E.L., Palacios, T.: 'Gate-First AlGaN/GaN HEMT Technology for High-Frequency Applications'*IEEE Electron Device Lett.*, 2009, **30**, (12), pp. 1254–1256.

[4] Ishida, H., Kajitani, R., Kinoshita, Y., *et al.*: 'GaN-based semiconductor devices for future power switching systems', in '2016 IEEE International Electron Devices Meeting (IEDM)' (IEEE, 2016), p. 20.4.1-20.4.4

[5] Nakajima, A., Sumida, Y., Dhyani, M.H., Kawai, H., Narayanan, E.M.: 'GaN-Based Super Heterojunction Field Effect Transistors Using the Polarization Junction Concept'*IEEE Electron Device Lett.*, 2011, **32**, (4), pp. 542–544.

[6] Nakajima, A., Nishizawa, S., Ohashi, H., *et al.*: 'One-chip operation of GaN-based P-channel and N-channel heterojunction field effect transistors', in '2014 IEEE 26th International Symposium on Power Semiconductor Devices & IC's (ISPSD)' (IEEE, 2014), pp. 241–244

[7] Nakajima, A., Liu, P., Ogura, M., *et al.*: 'Generation and transportation mechanisms for two-dimensional hole gases in GaN/AlGaN/GaN double heterostructures'*J. Appl. Phys.*, 2014, **115**, pp. 153707-1-153707–7.

[8] Kozodoy, P., Hansen, M., DenBaars, S.P., Mishra, U.K.: 'Enhanced Mg doping efficiency in Al0.2Ga0.8N/GaN superlattices'*Appl. Phys. Lett.*, 1999, **74**, (24), pp. 3681–3683.

[9] Nakajima, A., Liu, P., Ogura, M., *et al.*: 'Temperature-Independent Two-Dimensional Hole Gas Confined at GaN/AlGaN Heterointerface'*Appl. Phys. Express*, 2013, **6**, (9), pp. 91002-1-91002–4.

[10] Li, G., Wang, R., Song, B., *et al.*: 'Polarization-induced GaN-on-insulator E/D Mode p-channel heterostructure FETs'*IEEE Electron Device Lett.*, 2013, **34**, (7), pp. 852–854.

[11] Reuters, B., Hahn, H., Pooth, A., *et al.*: 'Fabrication of p-channel heterostructure field effect transistors with polarization-induced two-dimensional hole gases at metal – polar GaN/AlInGaN interfaces'*J.Phys. D Appl. Phys.*, 2014, **47**, pp. 175103-1-175103–10.

[12] Hahn, H., Reuters, B., Pooth, A., *et al.*: 'P-channel enhancement and depletion mode gan-based hfets with quaternary backbarriers'*IEEE Trans. Electron Devices*, 2013, **60**, (10), pp. 3005–3011.

[13] Yang, S., Huang, S., Schnee, M., Zhao, Q.-T., Schubert, J., Chen, K.J.: 'Fabrication and Characterization of Enhancement-Mode High-κ LaLuO3-AlGaN/GaN MIS-HEMTs'*IEEE Trans. Electron Devices*, 2013, **60**, (10), pp. 3040–3046.

[14] Kumar, A., De Souza, M.M.: 'Extending the bounds of performance in E-mode p-channel GaN MOSHFETs', in '2016 IEEE International Electron Devices Meeting (IEDM)' (IEEE, 2016), p. 7.4.1-7.4.4

[15] 'Silvaco TCAD Atlas' (Version V3.44.1R https://www.silvaco.com/products/tcad.html, 2017)

[16] Albrecht, J.D., Wang, R.P., Ruden, P.P., Farahmand, M., Brennan, K.F.: 'Electron transport characteristics of GaN for high temperature device modeling'*J. Appl. Phys.*, 1998, **83**, (9), p. 4777.

[17] Farahmand, M., Garetto, C., Bellotti, E., *et al.*: 'Monte Carlo simulation of electron transport in the III-nitride wurtzite phase materials system: binaries and ternaries'*IEEE Trans. Electron Devices*, 2001, **48**, (3), pp. 535–542.

[18] Nakajima, A., Sumida, Y., Dhyani, M.H., Kawai, H., Narayanan, E.M.S.: 'High Density Two-Dimensional Hole Gas Induced by Negative Polarization at GaN/AlGaN Heterointerface'*Appl. Phys. Express*, 2010, **3**, (12), pp. 121004-1-121004–3.

[19] Chen, J., Brewer, W.D.: 'Ohmic Contacts on p-GaN'*Adv. Electron. Mater.*, 2015, **1**, (8), pp. 1500113-1-1500113–7.

[20] Ambacher, O., Foutz, B., Smart, J., *et al.*: 'Two dimensional electron gases induced by spontaneous

and piezoelectric polarization in undoped and doped AlGaN/GaN heterostructures'*J. Appl. Phys.*, 2000, **87**, (1), p. 334.
[21] Hahn, H.: 'Threshold Voltage Engineering of GaN-based n-Channel and p-Channel Heterostructure Field Effect Transistors'. RWTH Aachen University, 2014
[22] Nakajima, A., Kubota, S., Kayanuma, R., *et al.*: 'Monolithic Integration of GaN-based Normally-off P- and N-channel MOSFETs', in '13th International Seminar on Power Semiconductors (ISPS'16)' (2016)
[23] Kub, F.J., Anderson, T.J., Koehler, A.D., Hobart, K.D.: 'Inverted p-channel III-nitride field effect transistor with hole carriers in the channel'. United States Patents, U.S. Patent No. 9,275,998, 2015
[24] Silvaco Inc.: 'Atlas User's Manual' (Silvaco International Software, Santa Clara, CA, USA, 2016)